Voxel-level comparison of arterial spin-labeled perfusion MRI and FDG-PET in Alzheimer disease

Y. Chen, PhD
D.A. Wolk, MD
J.S. Reddin, PhD
M. Korczykowski, MB, MA
P.M. Martinez, BA
E.S. Musiek, MD, PhD
A.B. Newberg, MD
P. Julin, MD, PhD
S.E. Arnold, MD
J.H. Greenberg, PhD
J.A. Detre, MD

Address correspondence and reprint requests to Dr. John A. Detre, Center for Functional Neuroimaging, University of Pennsylvania, 3W Gates Pavilion, 3400 Spruce St., Philadelphia, PA 19104
detre@mail.med.upenn.edu

ABSTRACT

Objective: We compared the ability of arterial spin labeling (ASL), an MRI method that measures cerebral blood flow (CBF), to that of FDG-PET in distinguishing patients with Alzheimer disease (AD) from healthy, age-matched controls.

Methods: Fifteen patients with AD (mean age 72 ± 6 years, Mini-Mental State Examination score [MMSE] 20 ± 6) and 19 age-matched controls (mean age 68 ± 6 years, MMSE 29 ± 1) underwent structural MRI. Participants were injected with 5 mCi of FDG during pseudocontinuous ASL scan, which was followed by PET scanning. Statistical parametric mapping and regions of interest (ROI) analysis were used to compare the ability of the 2 modalities in distinguishing patients from controls. Similarity between the 2 modalities was further assessed with linear correlation maps of CBF and metabolism to neuropsychological test scores.

Results: Good agreement between hypoperfusion and hypometabolism patterns was observed, with overlap primarily in bilateral angular gyri and posterior cingulate. ROI results showed similar scales of functional deficit between patients and controls in both modalities. Both ASL and FDG-PET were able to distinguish neural networks associated with different neuropsychological tests with good overlap between modalities.

Conclusions: Our voxel-wise results indicated that ASL-MRI provides largely overlapping information with FDG-PET. ROI analysis demonstrated that both modalities detected similar degrees of functional deficits in affected areas. Given its ease of acquisition and noninvasiveness, ASL-MRI may be an appealing alternative for AD studies. *Neurology*® 2011;77:1977–1985

GLOSSARY

Aβ = amyloid-β; **AD** = Alzheimer disease; **ADC** = Alzheimer's Disease Center; **ASL** = arterial spin labeling; **AUC** = area under the curve; **BNT** = Boston Naming Test; **CBF** = cerebral blood flow; **CDR** = Clinical Dementia Rating; **DSS** = Digit Symbol Substitution; **FDG-PET** = ^{18}fluoro-deoxyglucose PET; **FWHM** = full-width half maximum; **GM** = gray matter; **MCI** = mild cognitive impairment; **MMSE** = Mini-Mental State Examination; **MNI** = Montreal Neurological Institute; **MPRAGE** = magnetization-prepared rapid gradient echo; **MR** = magnetic resonance; **NACC** = National Alzheimer's Coordinating Center; **PSF** = point spread functions; **PVE** = partial volume effects; **rCBF** = relative cerebral blood flow; **rCMRGlc** = relative CMRGlc; **ROC** = receiver operating characteristic; **ROI** = region of interest; **SUV** = standardized uptake value; **TE** = echo time; **TIV** = total intracranial volume; **TR** = repetition time; **UDS** = Uniform Data Set; **VBM** = voxel-based morphometry; **WM** = white matter; **wsCV** = within-subject coefficient of variation.

Alzheimer disease (AD) is a neurodegenerative disorder associated with the accumulation of amyloid-β (Aβ) peptide and hyperphosphorylated tau protein, which lead to loss of neuronal and synaptic integrity and eventual cognitive decline.[1] Molecular markers (e.g., amyloid imaging) have limited capability in disease tracking and discriminating disease stages,[2,3] thus biomarkers sensitive to neurodegenerative changes may be better suited for these purposes.[4]

Structural MRI, probably the most developed quantitative methodology for measuring neurodegenerative change, has been consistently shown to correlate with disease severity.[5,6] Similarly, glucose metabolism (CMRGlc) measured by ^{18}fluoro-deoxyglucose PET (FDG-PET) correlates significantly with cognitive decline in AD.[3,7] Since CMRGlc reflects synaptic activ-

Supplemental data at www.neurology.org

Supplemental Data

From the Department of Neurology (Y.C., D.A.W., E.S.M., S.E.A., J.H.G., J.A.D.), Department of Radiology (J.S.R., A.B.N., J.A.D.), Department of Psychiatry (S.E.A.), Center for Functional Neuroimaging (D.A.W., M.K., J.H.G., J.A.D.), and Penn Memory Center (D.A.W., P.M.M., S.E.A.), University of Pennsylvania, Philadelphia; Department of Radiology (Y.C.), Center for Advanced MRI, Northwestern University, Chicago, IL; and AstraZeneca R&D (P.J.), Sodertalje, Sweden.

Study funding: Supported by the NIH (RR002305, NS058386, MH080729) and the Penn-AstraZeneca Alliance.

Disclosure: Author disclosures are provided at the end of the article.

ity,[8,9] which may precede structural changes, FDG-PET could be particularly sensitive in detecting disease-related functional changes and predicting decline, as evidenced in a recent study comparing multiple biomarkers that concluded FDG-PET was the most predictive for conversion from mild cognitive impairment (MCI) to AD.[10]

Regional cerebral blood flow (CBF) is generally tightly coupled to regional CMRGlc[11]; therefore, it may provide similar information to FDG-PET. Arterial spin labeling (ASL) is an MRI methodology that uses endogenous arterial blood water as a tracer to quantify CBF. Its noninvasive nature and high reproducibility over time[12] make it an attractive and potentially cost-effective alternative to FDG-PET.

Though patterns of hypoperfusion in limited ASL studies largely recapitulate hypometabolism patterns reported with FDG-PET (for review, see reference [13]), no direct comparison between the methodologies for AD exists. Here, we compare the ability of ASL and FDG-PET to distinguish patients with AD from controls.

Table 1 Demographic and neuropsychological summary of subjects included in the current study[a]

	Controls (n = 19)	Patients with AD (n = 15)
Age, y	69.2 (7.6)	72.0 (6.3)
Education, y[b]	17.2 (2.6)	14.8 (2.8)
% Female[c]	63	60
APOE ϵ4 carrier, %[c]	33	75
MMSE[d]	29.5 (1.0)	19.9 (5.9)
CDR–sum of boxes[d]	0 (0)	5.4 (3.3)
Neuropsychological testing		
Animal fluency[d]	22.9 (4.9)	10.1 (3.7)
Boston Naming Test[d]	29.1 (1.1)	20.2 (5.8)
Digit Span Forward[b]	9.1 (1.8)	7.4 (2.1)
Digit Span Backward[d]	8.0 (2.7)	4.5 (1.7)
Digit Symbol Substitution[d]	53.4 (10.5)	24.9 (11.0)
Word-List Memory Test[d]	25.9 (2.5)	9.2 (4.4)
Delayed Word-List Recall[d]	9.2 (1.2)	0.9 (1.4)
Word-List Recognition[d]	3.3 (0.1)	1.4 (1.0)

Abbreviations: AD = Alzheimer disease; CDR = Clinical Dementia Rating; MMSE = Mini-Mental State Examination.
[a] Data are presented as mean (SD).
[b] $p < 0.05$.
[c] $p < 0.05$ for χ^2 test applied to gender and *APOE* ϵ4 carriers.
[d] $p < 0.001$ for 2-sample *t* test between patients and controls.

METHODS **Subjects.** Seventeen patients with probable AD based on the National Institute of Neurological and Communicative Disorders and Stroke–Alzheimer's Disease and Related Disorders Association criteria[14] were recruited from the University of Pennsylvania's Alzheimer's Disease Center (ADC) for the current study. As part of their enrollment in the ADC, all patients undergo an extensive neuropsychological evaluation, including all components of the National Alzheimer's Coordinating Center's (NACC) Uniform Data Set (UDS),[15] which is repeated annually. All patients had a MMSE score 25 or lower and a Clinical Dementia Rating (CDR) global score of 0.5 or higher. Two patients did not complete the imaging protocol and were excluded from the final analysis. Nineteen age-matched healthy controls, with MMSE >26 and CDR global score of 0, were recruited by advertisement. A summary of the demographic characteristics and neuropsychological test results is shown in table 1. Raw test scores are reported for all tests except Word-List Recognition, where d′ was calculated to account for false alarms.[16]

Standard protocol approvals, registrations, and patient consents. The study protocol was approved by the local institutional review board and written informed consent was obtained from all subjects or their legally designated representatives prior to the study.

Imaging protocol. ***MRI.*** MRIs were acquired on a 3-T whole-body Siemens TIM Trio scanner (Erlangen, Germany) with an 8-channel receive-only head coil and body coil transmission. High-resolution whole brain anatomic images were collected using 3-dimensional magnetization-prepared rapid gradient echo (MPRAGE) with the following parameters: inversion time = 950 msec, echo time (TE)/repetition time (TR) = 3.87 msec/1,620 msec, 160 axial slices, 1 mm isotropic resolution. Resting CBF measurements were acquired using pseudocontinuous ASL[17] with labeling duration and postlabeling delay of 1.5 s each. The labeling plane was positioned 90 mm below the center of the imaging slab composed of 18 axial slices (6 mm thickness, 1.2 mm gap). Fifty-nine pairs of interleaved control and tag images were acquired using gradient-echo echoplanar imaging with TR/TE = 4 s/17 msec and voxel resolution of $3.5 \times 3.5 \times 6$ mm^3, which lasted 8 minutes. Three ASL scans were acquired and concatenated during data analysis to improve signal-to-noise ratio.

A subset of 9 patients was rescanned with MRI approximately 1 week after the first scan session to assess test-retest reproducibility of ASL. The rescan session consisted of the same MPRAGE structural scan, as well as 2 ASL scans as described above.

PET imaging. To minimize physiologic changes between the magnetic resonance (MR) and PET scans, 5 mCi of FDG was injected via an IV catheter while the subject was in the MR scanner, allowing FDG uptake to occur during MR acquisition.[18] At the end of the MRI session, subjects were transported to the PET scanner and images were acquired based on the ADNI PET imaging protocol[19] on an Allegro scanner (Philips). Images were obtained over a 30-minute period followed by a

transmission scan for attenuation correction. At the completion of the scanning, the images were reconstructed in the transaxial planes into voxels of dimension $2 \times 2 \times 2$ mm^3 using an iterative reconstruction process.[20]

Image processing. All images were processed using Statistical Parametric Mapping (SPM5, Wellcome Department of Imaging Neuroscience, London, UK) and customized MATLAB scripts (The Mathworks Inc., Natick, MA). To account for the enlarged ventricles and atrophied gray matter (GM) typical of elderly subjects, an age-specific template was used for spatial normalization. Voxel-wise statistics were generated by comparing 1) MPRAGE, 2) ASL, and 3) PET images between patients and controls to detect AD-related atrophy, hypoperfusion, and hypometabolism patterns, respectively. All results were thresholded at $p < 0.05$ with false discovery rate correction for multiple comparisons and cluster threshold of 50 voxels unless otherwise specified. Detailed processing steps for the 3 image types are discussed below.

MPRAGE images. The MPRAGE images were processed using optimized voxel-based morphometry (VBM).[21] Briefly, the images were first segmented into GM, white matter (WM), and CSF using tissue priors from an age-specific template in Montreal Neurological Institute (MNI) space. These tissue probability maps were used to generate normalization parameters for spatial normalization of the unsegmented MPRAGE images. The spatially normalized MPRAGE images were segmented again and the tissue probability maps were modulated to account for volume changes during nonlinear spatial normalization. Total intracranial volume (TIV) was calculated by thresholding these tissue probability maps at 0.5, summing the above-threshold voxels and multiplying by the voxel volume. The modulated GM probability maps were finally smoothed by a 12-mm full-width half maximum (FWHM) kernel and entered into a 2-sample *t* test with age, years of education, and TIV as covariates to detect GM volume changes in patients.

ASL images. Raw images from the ASL scans were first coregistered to the MPRAGE images of the same session and motion-corrected using a 6-parameter rigid body spatial transformation. Pairwise subtraction images were then generated and images with signal spikes caused by motion artifacts were removed according to previously published criteria.[22] Averaged difference images were converted to mL/100 g/min using a single-compartment model[23] (see figure e-1a on the *Neurology*® Web site at www.neurology.org for sample CBF maps).

The low resolution of the CBF images necessitates correction of partial volume effects (PVE) as it interferes with the accuracy of CBF quantification and subsequent comparisons. High-resolution GM and WM probability maps generated from each subject's MPRAGE images were first smoothed with a $4 \times 4 \times 6$ mm^3 kernel to mimic the PVE of the ASL images. These smoothed tissue maps were then subsampled to the resolution of the CBF images and thresholded at >0.3 to minimize division artifacts, before being applied to the CBF images for PVE correction using the equation $I_{corrected} = I_{uncorrected}/(P_{GM} + 0.4\,P_{WM})$, where the 0.4 factor is the global ratio between WM and GM,[24] and P_{GM} and P_{WM} are the probabilities of GM and WM, respectively. The PVE-corrected CBF images were spatially normalized to MNI space using the same normalization parameters calculated from the high-resolution GM probability maps. Global effects were eliminated by dividing the images by each subject's mean whole brain CBF.

Patient test-retest reproducibility for ASL was assessed using within-subject coefficient of variation (wsCV),[25] defined as $wsCV = 100 \times \sigma/\mu$, where σ is the SD of the test-retest difference and μ is the mean of test-retest scans. wsCV values were calculated for global GM, hippocampus, and a composite ROI using coordinates of the 5 most frequently cited regions (left and right angular gyri, left and right posterior cingulate, and left middle/inferior temporal gyrus) sensitive to AD and MCI in FDG-PET studies developed by Landau et al.[7]

PET images. Raw count FDG-PET images were converted to standardized uptake value (SUV) images (sample images in figure e-1b) using the SUV scale factor in the dicom header. After coregistration to the anatomic MRI, the same partial volume correction procedure as described for the ASL data above was applied to the SUV images. To address the different point spread functions (PSF) of ASL and PET, the high-resolution tissue probability maps were smoothed by the PET PSF of $5.5 \times 5.5 \times 5.6$ mm^3 before being resliced to the image space of the FDG-PET images for PVE correction. The PVE-corrected FDG-PET images were spatially and intensity normalized in a similar fashion as the ASL images.

Statistical analysis. The PVE-corrected, spatially and intensity normalized ASL and FDG-PET images were smoothed with a 12-mm 3-dimensional kernel, then analyzed using a 2×2 factorial design with condition (patient and control) and modality (ASL and FDG-PET) as the 2 factors, and age and years of education as covariates. To limit the analysis to GM, a mean GM mask was generated by thresholding each subject's spatially normalized GM probability map to 0.2 or above. Only voxels considered as cortical GM for all subjects were included in the mask. Maps of hypoperfusion and hypometabolism were generated using within-modality *t* contrasts between patient and control groups. Further investigation of the degree of overlap and discrepancy between the 2 modalities was achieved using conjunction analysis and an F-contrast representing modality × condition interaction.

To support the voxel-based analysis, a ROI analysis was also performed using the composite ROI described above[7] given the sensitivity of these regions to CMRGlc changes associated with early AD. Additionally, bilateral angular gyri, posterior cingulate, thalamus, motor cortex, and basal ganglia ROIs generated from Automated Anatomic Labeling[26] in SPM were also used to extract relative CBF (rCBF) and relative CMRGlc (rCMRGlc) values. The angular, posterior cingulate, and composite ROIs were used to compare the degree of functional deficit in patients for both modalities, while the latter 3 of the aforementioned ROIs have been found to be less vulnerable to functional changes in AD and are expected to have minimal difference between patient and control groups.

In order to determine whether resting state metabolism and CBF similarly correlated with neuropsychological performance and to demonstrate the overlap in brain–behavior relationships between the 2 methodologies, ASL and FDG-PET images from all subjects were entered into a linear regression model with each of the neuropsychological test scores in table 1 as the regressor, and age and years of education as nuisance covariates. Correlation results were statistically thresholded at $p < 0.005$ uncorrected and clusters of 50 voxels or more.

RESULTS The mean ± SD CBF values for whole brain GM, hippocampus, and composite ROI were 38.2 ± 7.0, 42.6 ± 9.4, and 22.4 ± 4.3 mL/100 g/min for scan 1 and 44.8 ± 11.7, 45.5 ± 11.0, and 26.6 ± 7.9 mL/100 g/min for scan 2. The corre-

Figure 1 Results of voxel-wise statistics between patients and controls

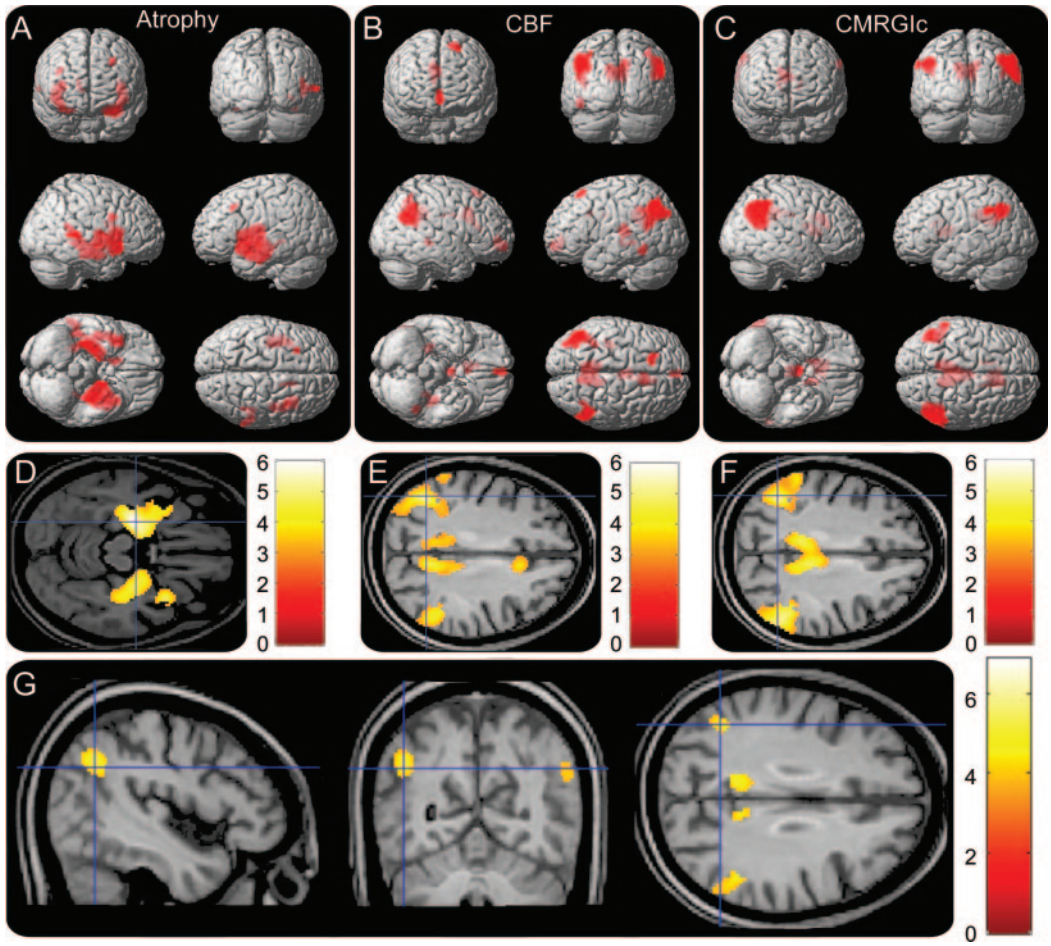

Areas of (A) atrophy, (B) hypoperfusion, and (C) hypometabolism rendered onto 3-dimensional brains, with color intensity representing depth from brain surface. Red represents Alzheimer disease–related decreases. Representative slices with color bar representing range of *t* values are shown in (D–F). (G) Results of conjunction analysis showing areas of overlap between hypoperfusion and hypometabolism. All images were statistically thresholded at $p < 0.05$, false discovery rate correction for multiple comparison, cluster >50. No increases in gray matter volume, cerebral blood flow (CBF), or CMRGlc were detected.

sponding wsCV ± 95% confidence interval values were 16% ± 1%, 16% ± 2%, and 18% ± 4%. Both GM and hippocampus had similar CBF and wsCV values, whereas the composite ROI had lower CBF, likely due to the inclusion of the inferior temporal lobes, areas that typically suffer from signal loss due to high static magnetic field inhomogeneity. As a result of the lower CBF, wsCV for the composite ROI was slightly elevated.

Voxel-wise statistical analysis results of patients compared to controls are shown in figure 1. AD-related (A) GM atrophy, (B) hypoperfusion, and (C) hypometabolism patterns are rendered onto 3-dimensional brains, where color intensity represents depth. Figure 1, D–F, shows a representative slice with a color bar representing the scale of the *t* values. The atrophy results closely resemble the typical AD atrophy pattern, primarily localized to the temporal lobe. The hypoperfusion and hypometabolism results, on the other hand, were localized to the bilateral angular gyri and posterior cingulate. Excellent agreement between the hypoperfusion and hypometabolism maps was confirmed by conjunction analysis (figure 1G), which revealed significant overlap between ASL and FDG-PET in the bilateral angular gyri and posterior cingulate. No significant modality × condition interaction was detected at the statistical threshold used. A summary of the regions detected, together with the MNI coordinates, maximum *z* scores, and number of voxels, is shown in table 2.

Figure 2 shows bar plots of (A) rCBF and (B) rCMRGlc values for the various ROIs, with data from controls in dark green and those from patients in pale green. Error bars represent standard errors. Two-sample *t* tests revealed that patient rCBF and rCMRGlc were significantly lower in the angular, composite, and posterior cingulate ROIs ($p <$

Table 2 Summary of voxel-wise comparisons between patients and controls

Anatomic label	x, y, z (mm) coordinates	*Z* score	Voxels
Atrophy			
Right hippocampus	32 −36 −2	4.78	879
Left insula	−26 −14 −14	4.68	2,666
Right insula	40 12 −12	4.22	1,397
Right caudate	12 10 12	4.18	123
Right inferior frontal operculum	38 6 26	3.74	72
Left middle frontal gyrus	−26 20 38	3.67	53
ASL			
Left and right precuneus	−12 −52 26	6.05	1,208
Left angular gyrus	−44 −62 36	4.84	1,124
Right angular gyrus	44 −50 28	4.54	870
Right mid cingulate	10 14 28	4.16	409
Left inferior temporal gyrus	−46 −50 −10	3.94	101
Left Heschl gyrus	−34 −28 14	3.83	190
Left medial orbitofrontal	0 58 −6	3.50	226
Left superior frontal	−16 24 62	3.41	86
PET			
Right mid-cingulate	−10 −50 24	5.97	2,130
Right angular gyrus	58 −64 32	5.47	2,225
Left angular gyrus	−44 −50 36	5.18	1,301
Right thalamus	2 −12 −4	5.11	411
Left caudate	−8 6 8	4.48	112
Right caudate	12 12 12	4.23	150
Left middle frontal	−28 22 38	3.94	52
Left Heschl gyrus	−32 −30 14	3.81	93
Right inferior frontal operculum	58 20 26	3.60	68
Left inferior temporal gyrus	−62 −20 −30	3.57	131
Right Heschl gyrus	48 −18 10	3.25	98
Left medial superior frontal	0 46 24	3.22	170
Left middle temporal	−68 −24 −6	3.17	133
Conjunction			
Left posterior cingulate	−10 −50 24	5.91	434
Left angular gyrus	−44 −62 −36	4.83	392
Right angular gyrus	44 −50 30	4.30	457
Right anterior cingulate	8 14 26	4.07	70

0.005). Cohen *d* effect size was 2.05 for rCBF and 1.92 for rCMRGlc in the composite ROI, demonstrating similar sensitivity for discrimination of patients with AD from controls. Receiver operating characteristic (ROC) curves constructed using the rCBF and rCMRGlc values extracted from the composite ROI are shown in figure e-2. The areas under the curve (AUC) were 0.94 and 0.92 for rCBF and rCMRGlc, respectively.

Results of partial correlation between CBF and CMRGlc with Boston Naming Test (BNT) and Digit Symbol Substitution (DSS) scores are rendered onto 3-dimensional brains in figure 3, revealing significant overlap between the 2 methodologies. Red and green represent positive and negative correlations with the test scores. For BNT, positive correlations include the ventrolateral prefrontal cortex and inferior and middle temporal lobes. Alternatively, DSS had a different pattern involving positive correlations in the dorsolateral prefrontal cortex and bilateral inferior parietal lobes. Similar overlap between the methodologies was observed for correlations with other psychometric variables (see figure e-3).

DISCUSSION FDG-PET has proven to be a useful tool in both the clinical arena and in research studies of AD. This methodology holds particular promise as an early marker of functional change, which may have important prognostic value in preclinical disease and for tracking outcomes in therapeutic intervention trials.[4] Mounting evidence for the utility of various MRI measures such as structural imaging, white matter hyperintensities, and diffusion tensor imaging has established MRI to be a powerful tool for studying AD,[13] but PET remains the gold standard for functional assessments. An MRI-based functional measurement such as ASL could potentially streamline AD studies as it can be easily incorporated into any MRI protocol.

The primary goal of this study was to compare the abilities of ASL-MRI and FDG-PET in detecting functional abnormalities associated with AD. As is evident in figure 1, both ASL and FDG-PET identified the typical AD pattern of compromised function in the bilateral parietal lobes and the posterior cingulate.[19] Conjunction analysis showed that the overlap between the 2 modalities in these areas was statistically significant. Contrary to several reports of hyperperfusion in the hippocampus for patients with prodromal AD,[27–29] we did not find any areas with mismatched CBF and CMRGlc, suggesting that the elevated hippocampal CBF was likely a compensatory mechanism only present in early disease stages. Complementary to the voxel-wise comparison, the ROI results showed significantly lower rCBF and rCMRGlc in the angular and posterior cingulate areas of the patients, while motor, thalamus, and basal ganglia regions were unaffected. ROC analysis on the ROI results demonstrated high disease detection accuracy of >0.9 for both modalities. While promising, this preliminary result requires further validation in a larger scale study. Nonetheless, both ROI and voxel-wise results support the notion that ASL and FDG-PET offer similar functional measures.

Figure 2 Bar plots of (A) relative cerebral blood flow (rCBF) and (B) CMRGlc (rCMRGlc) extracted from regions of interest (ROIs)

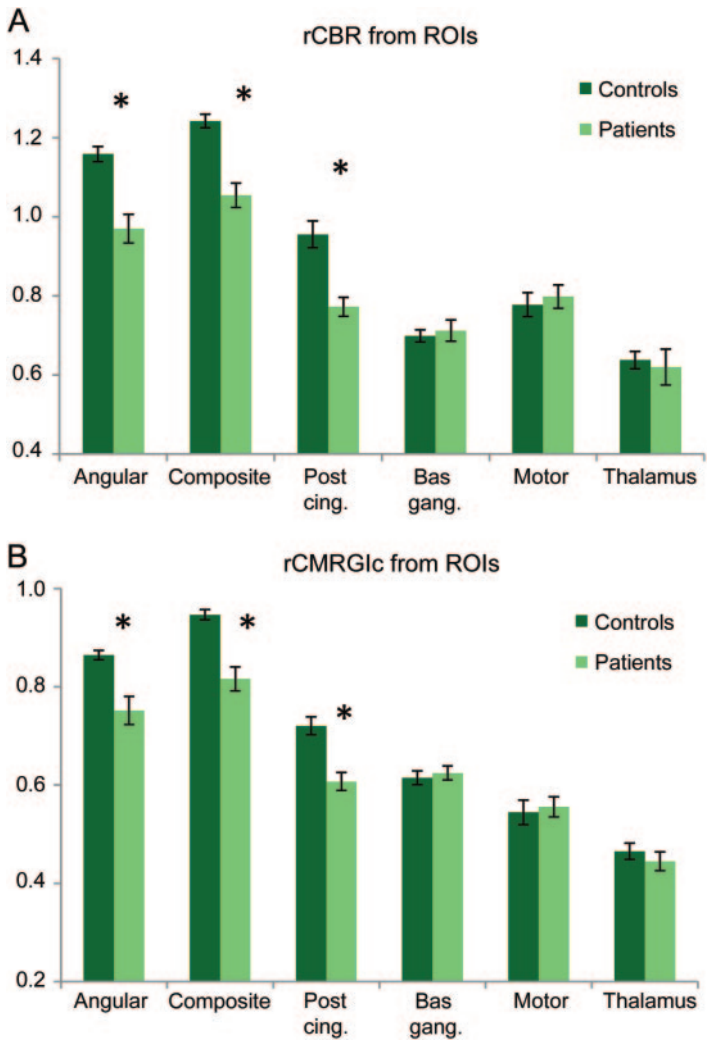

Both rCBF and rCMRGlc show similar degrees of functional deficit between control and patients in affected areas, which were statistically significant at $p < 0.005$ (*). Cohen *d* value was 2.05 for rCBF and 1.92 for rCMRGlc extracted from the composite ROI.

The AD-related atrophy pattern was significantly different from the hypoperfusion and hypometabolism patterns (figure e-4). This frequently reported discrepancy[30,31] has been suggested to be a result of diaschisis, in which in addition to local neuronal loss, functional deficits can also occur in distant areas as a result of denervation.[32] In support of this theory, Villain et al.[33] reported a strong correlation between hippocampal atrophy and cingulum bundle disruption, which was in turn correlated to hypometabolism in association cortices. The complementary findings associated with structural and functional measures (CMRGlc and CBF) suggest a value in obtaining both structural and functional data in tracking disease progression, which can be easily achieved with MRI techniques such as ASL and MPRAGE.

The mean GM CBF value in patients was approximately 20% lower than that of the controls in the current study (mean ± SD = 49.9 ± 10.1 mL/100 g/min), in good agreement with previous studies reporting global hypoperfusion in patients with AD.[34] Compared to the majority of reproducibility studies on ASL, our wsCV of 16% is slightly higher than the norm of less than 10%.[12,35] This is likely due to the fact that most other studies were performed in young, healthy subjects, who typically have higher CBF and also better signal-to-noise ratio in their ASL scans.[36] Though no formal assessment of FDG-PET reproducibility in patients with AD exist, CMRGlc measurements in healthy subjects have a reproducibility of 7.1%,[37] which is slightly better than the reproducibility of ASL in healthy subjects.

Both ASL and FDG-PET show expected correlations with cognitive task performance, as evidenced by the correlation maps for BNT and DSS in figure 3. While not a central goal of this present study, the inferior frontal/temporal correlation with BNT and dorsal frontoparietal correlation with DSS are consistent with known networks supporting naming and control/working memory processes involved in these psychometric measures.[38,39] That ASL and FDG-PET were able to detect these distinct networks with good agreement between them is further evidence for the similarity between these 2 methodologies. A major limitation of the present study is the small patient cohort, which precludes assessment of correlations with disease severity. Further research in a larger patient population of more varied disease stages is necessary to determine the utility of ASL in tracking disease severity.

Using voxel-wise comparisons, we have demonstrated that ASL-MRI identifies highly overlapping patterns of hypoperfusion with FDG-PET hypometabolism in patients with AD compared to controls. ROI results revealed that rCBF and rCMRGlc show similar degrees of functional deficits between patients and controls in affected brain regions. The noninvasive nature of ASL makes it well-suited for screening and longitudinal disease tracking. However, its sensitivity in early-stage AD remains to be investigated. In order to facilitate planning of ASL-MRI longitudinal studies, we also present an estimate for ASL-MRI reproducibility in our patient population. Future work in a more varied patient cohort will help realize the full potential of ASL-MRI in AD-related research and clinical care.

Figure 3 Cerebral blood flow (CBF) and CMRGlu correlation maps with neurosychological test scores

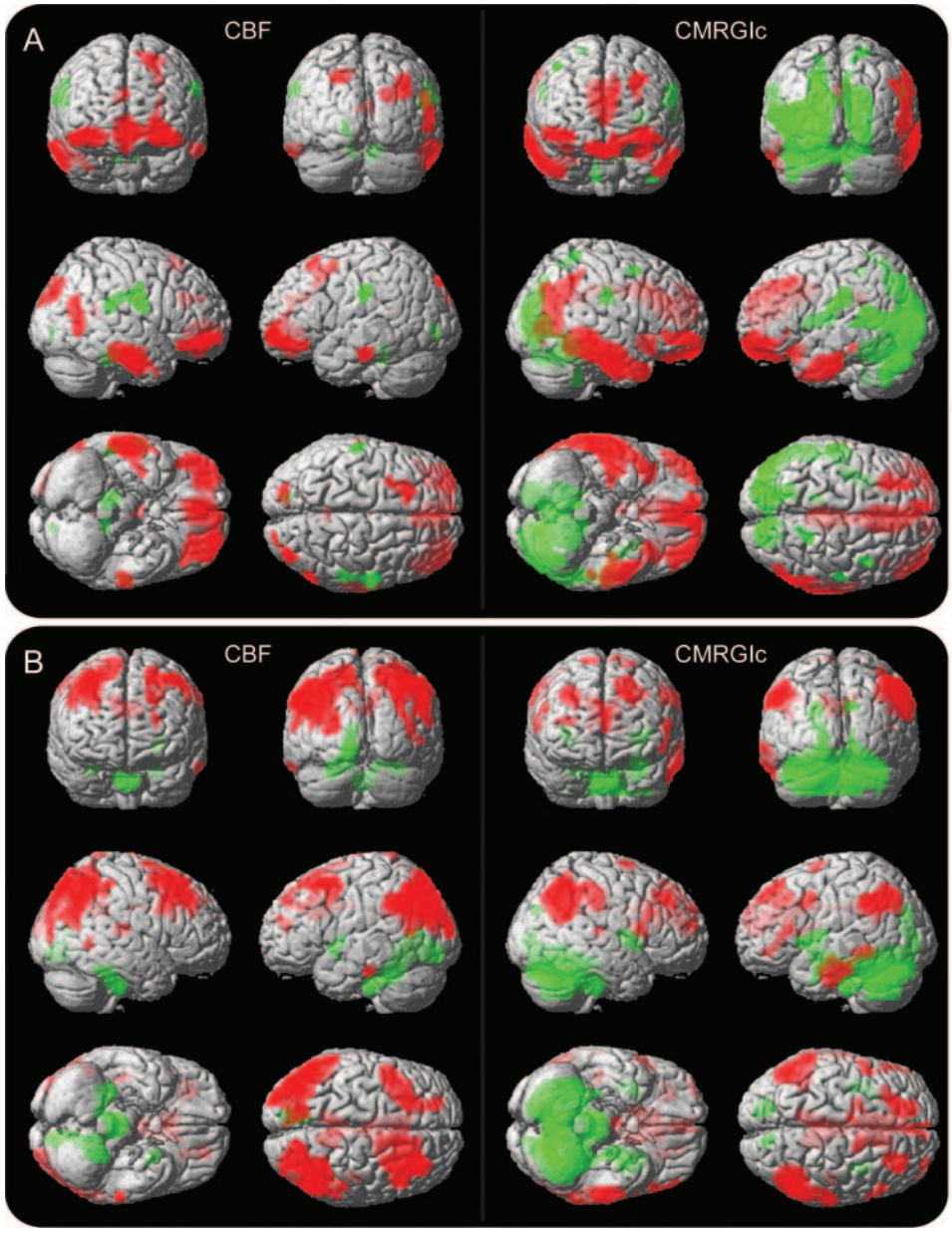

(A) Correlation between CBF (left) and CMRGlu (right) with Boston Naming Test scores. (B) Correlation between CBF (left) and CMRGlu (right) with Digit Symbol Substitution scores. Red and green represent positive and negative correlations respectively. Color intensity represents depth from brain surfaces. Statistical images were thresholded at $p < 0.005$, uncorrected for multiple comparisons, cluster size >50.

AUTHOR CONTRIBUTIONS

Manuscript preparation: Y.C., D.A.W., J.A.D. Data analysis/interpretation: Y.C., D.A.W., E.M., J.A.D. Study concept/design: A.B.N., P.J., S.E.A., J.G., J.A.D. Patient recruitment/evaluation and data acquisition: M.K., P.M.M., J.S.R.

ACKNOWLEDGMENT

The authors acknowledge the assistance of Nancy Wintering in coordinating the PET scans for this study. The authors also thank Brian B. Avants for supplying the age-specific template.

DISCLOSURE

Dr. Chen reports no disclosures. Dr. Wolk serves as a consultant for GE Healthcare; and receives/has received research support from GE Healthcare, Pfizer Inc, the NIH, and the PA Department of Health. Dr. Reddin has received funding for travel and speaker honoraria from Janssen. M. Korczykowski, P.M. Martinez, and Dr. Musiek report no disclosures. Dr. Newberg receives research support from the NIH. Dr. Julin is a full-time employee of AstraZeneca. Dr. Arnold serves on a scientific advisory board for Eli Lilly and Company; serves on the editorial boards of *Translational Neuroscience* and *Schizophrenia Bulletin*; serves as a consultant for the Cowen Group; and receives research support from Eli Lilly and Company, Pfizer Inc, Janssen, Neuronetrix, Johnson & Johnson, the NIH, and the Marian S. Ware Family Foundation. Dr. Greenberg serves on the editorial board of the *Journal of Cerebral Blood Flow and Metabolism*; has a patent pending re: Use of diffuse correlation spectroscopy for the non-invasive measurement of cerebral blood flow; and receives research support from the NIH/NINDS and the Institute for Translational Medicine and Therapeutics (University of Pennsylvania). Dr. Detre serves on a scientific

advisory board of Pittsburgh NMR Center; serves as an Associate Editor of the *Journal of Neuroimaging*; serves as a consultant for Pfizer Inc; receives research support from Wyeth, AstraZeneca, Pfizer Inc, the National Science Foundation, and the NIH; is an inventor on a patent re: ASL perfusion MRI and receives royalties from the University of Pennsylvania for its licensure; and has acted as a witness or consultant in legal proceedings.

Received April 25, 2011. Accepted in final form August 12, 2011.

REFERENCES

1. Braak H, Braak E. Neuropathological stageing of Alzheimer-related changes. Acta Neuropathol 1991;82:239–259.
2. Jack CR Jr, Lowe VJ, Senjem ML, et al. ^{11}C PiB and structural MRI provide complementary information in imaging of Alzheimer's disease and amnestic mild cognitive impairment. Brain 2008;131:665–680.
3. Jagust WJ, Landau SM, Shaw LM, et al. Relationships between biomarkers in aging and dementia. Neurology 2009;73:1193–1199.
4. Jack CR, Jr., Knopman DS, Jagust WJ, et al. Hypothetical model of dynamic biomarkers of the Alzheimer's pathological cascade. Lancet Neurol 2010;9:119–128.
5. Jack CR, Jr., Lowe VJ, Weigand SD, et al. Serial PIB and MRI in normal, mild cognitive impairment and Alzheimer's disease: implications for sequence of pathological events in Alzheimer's disease. Brain 2009;132:1355–1365.
6. Vemuri P, Wiste HJ, Weigand SD, et al. MRI and CSF biomarkers in normal, MCI, and AD subjects: predicting future clinical change. Neurology 2009;73:294–301.
7. Landau SM, Harvey D, Madison CM, et al. Associations between cognitive, functional, and FDG-PET measures of decline in AD and MCI. Neurobiol Aging 2011;32:1207–1218.
8. Schwartz WJ, Smith CB, Davidsen L, et al. Metabolic mapping of functional activity in the hypothalamo-neurohypophysial system of the rat. Science 1979;205:723–725.
9. Attwell D, Laughlin SB. An energy budget for signaling in the grey matter of the brain. J Cereb Blood Flow Metab 2001;21:1133–1145.
10. Landau SM, Harvey D, Madison CM, et al. Comparing predictors of conversion and decline in mild cognitive impairment. Neurology 2010;75:230–238.
11. Jueptner M, Weiller C. Review: does measurement of regional cerebral blood flow reflect synaptic activity? Implications for PET and fMRI. Neuroimage 1995;2:148–156.
12. Chen Y, Wang DJ, Detre JA. Test-retest reliability of arterial spin labeling with common labeling strategies. J Magn Reson Imaging 2011;33:940–949.
13. Alsop DC, Dai W, Grossman M, Detre JA. Arterial spin labeling blood flow MRI: its role in the early characterization of Alzheimer's disease. J Alzheimers Dis 2010;20:871–880.
14. McKhann G, Drachman D, Folstein M, Katzman R, Price D. Clinical diagnosis of Alzheimer's disease: report of the NINCDS-ADRDA Work Group under the auspices of Department of Health and Human Services Task Force on Alzheimer's Disease. Neurology 1984;34:285–297.
15. Morris JC, Weintraub S, Chui HC, et al. The Uniform Data Set (UDS): clinical and cognitive variables and descriptive data from Alzheimer Disease Centers. Alzheimer Dis Assoc Disord 2006;20:210–216.
16. Wolk DA, Dickerson BC. Apolipoprotein E (APOE) genotype has dissociable effects on memory and attentional-executive network function in Alzheimer's disease. Proc Natl Acad Sci USA 2010;107:10256–10261.
17. Dai W, Garcia D, de Bazelaire C, Alsop DC. Continuous flow-driven inversion for arterial spin labeling using pulsed radio frequency and gradient fields. Magn Reson Med 2008;60:1488–1497.
18. Newberg AB, Wang J, Rao H, et al. Concurrent CBF and CMRGlc changes during human brain activation by combined fMRI-PET scanning. Neuroimage 2005;28:500–506.
19. Jagust WJ, Bandy D, Chen K, et al. The Alzheimer's Disease Neuroimaging Initiative positron emission tomography core. Alzheimers Dement 2010;6:221–229.
20. Chang L-T. A method for attenuation correction in radionuclide computed tomography. IEEE Trans Nucl Sci 1978;25:638–643.
21. Good CD, Johnsrude IS, Ashburner J, Henson RN, Friston KJ, Frackowiak RS. A voxel-based morphometric study of ageing in 465 normal adult human brains. Neuroimage 2001;14:21–36.
22. Wang Z, Aguirre GK, Rao H, et al. Empirical optimization of ASL data analysis using an ASL data processing toolbox: ASLtbx. Magn Reson Imaging 2008;26:261–269.
23. Wang J, Alsop DC, Song HK, et al. Arterial transit time imaging with flow encoding arterial spin tagging (FEAST). Magn Reson Med 2003;50:599–607.
24. Du AT, Jahng GH, Hayasaka S, et al. Hypoperfusion in frontotemporal dementia and Alzheimer disease by arterial spin labeling MRI. Neurology 2006;67:1215–1220.
25. Bland JM, Altman DG. Measurement error proportional to the mean. BMJ 1996;313:106.
26. Tzourio-Mazoyer N, Landeau B, Papathanassiou D, et al. Automated anatomical labeling of activations in SPM using a macroscopic anatomical parcellation of the MNI MRI single-subject brain. Neuroimage 2002;15:273–289.
27. Alsop DC, Casement M, de Bazelaire C, Fong T, Press DZ. Hippocampal hyperperfusion in Alzheimer's disease. Neuroimage 2008;42:1267–1274.
28. Dai W, Lopez OL, Carmichael OT, Becker JT, Kuller LH, Gach HM. Mild cognitive impairment and Alzheimer disease: patterns of altered cerebral blood flow at MR imaging. Radiology 2009;250:856–866.
29. Fleisher AS, Podraza KM, Bangen KJ, et al. Cerebral perfusion and oxygenation differences in Alzheimer's disease risk. Neurobiol Aging 2009;30:1737–1748.
30. Chetelat G, Desgranges B, Landeau B, et al. Direct voxel-based comparison between grey matter hypometabolism and atrophy in Alzheimer's disease. Brain 2008;131:60–71.
31. Matsuda H, Kitayama N, Ohnishi T, et al. Longitudinal evaluation of both morphologic and functional changes in the same individuals with Alzheimer's disease. J Nucl Med 2002;43:304–311.
32. Jobst KA, Smith AD, Barker CS, et al. Association of atrophy of the medial temporal lobe with reduced blood flow in the posterior parietotemporal cortex in patients with a clinical and pathological diagnosis of Alzheimer's disease. J Neurol Neurosurg Psychiatry 1992;55:190–194.
33. Villain N, Desgranges B, Viader F, et al. Relationships between hippocampal atrophy, white matter disruption, and gray matter hypometabolism in Alzheimer's disease. J Neurosci 2008;28:6174–6181.

34. Alavi A, Newberg AB, Souder E, Berlin JA. Quantitative analysis of PET and MRI data in normal aging and Alzheimer's disease: atrophy weighted total brain metabolism and absolute whole brain metabolism as reliable discriminators. J Nucl Med 1993;34:1681–1687.
35. Petersen ET, Mouridsen K, Golay X. The QUASAR reproducibility study, part II: results from a multi-center arterial spin labeling test-retest study. Neuroimage 2010;49:104–113.
36. Xu G, Rowley HA, Wu G, et al. Reliability and precision of pseudo-continuous arterial spin labeling perfusion MRI on 3.0 T and comparison with 15O-water PET in elderly subjects at risk for Alzheimer's disease. NMR Biomed 2010;23:286–293.
37. Camargo EE, Szabo Z, Links JM, Sostre S, Dannals RF, Wagner HN, Jr. The influence of biological and technical factors on the variability of global and regional brain metabolism of 2-[18F]fluoro-2-deoxy-D-glucose. J Cereb Blood Flow Metab 1992;12:281–290.
38. Amici S, Ogar J, Brambati SM, et al. Performance in specific language tasks correlates with regional volume changes in progressive aphasia. Cogn Behav Neurol 2007;20:203–211.
39. Venkatraman VK, Aizenstein H, Guralnik J, et al. Executive control function, brain activation and white matter hyperintensities in older adults. Neuroimage 2010;49:3436–3442.

Take Your Seat at the Table! Apply for 2012 Neurology on the Hill

AAN members in the United States are encouraged to apply for Neurology on the Hill to be held February 27–28, 2012, in Washington, DC. Participants will learn about the Academy's top advocacy priorities and receive the training they need to present neurology's position on leading health policy issues to their senators, representatives, and congressional staff members.

Applications for the event are due by December 11, 2011. Neurology on the Hill is open to all US members of the AAN excluding medical students. The AAN will pay for airfare and hotel. For more information or to apply, visit *www.aan.com/view/2012NOH*, or contact Julie Grengs at *jgrengs@aan.com* or (651) 695-2755.

Call for Submissions: *Neurology* launches Global Perspectives!

In October 2011, *Neurology*® will launch Global Perspectives, an expanded and enhanced version of the International Newsletter. New Co-Editors Johan A. Aarli, MD, and Oded Abramsky, MD, PhD, FRCP, encourage submissions to this section that will provide a platform in *Neurology* for publishing news about scientific findings or academic issues. News may include international research content, spotlights on specific neurologic practice concerns within a country, or important information about international educational or scientific collaborative efforts.

Submissions must be 1,250 words or less with five or less references. A maximum of two figures or two tables (or combination) can be incorporated if necessary. For complete submission requirements, please go to *www.neurology.org* and click on "Information for Authors." The submissions will be reviewed by the editors and may be edited for clarity.

Interested submitters can register and upload manuscripts under the section "Global Perspectives" at *http://submit.neurology.org*. Please send inquiries to Kathy Pieper, Managing Editor, *Neurology; kpieper@neurology.org*.